European Journal of Nuclear Medicine and Molecular Imaging (2019) 46:1889–1901
https://doi.org/10.1007/s00259-019-04384-7

ORIGINAL ARTICLE

Differentiation of treatment-related changes from tumour progression: a direct comparison between dynamic FET PET and ADC values obtained from DWI MRI

Jan-Michael Werner[1] · Gabriele Stoffels[2] · Thorsten Lichtenstein[3] · Jan Borggrefe[3] · Philipp Lohmann[2] · Garry Ceccon[1] · Nadim J. Shah[2,4] · Gereon R. Fink[1,2] · Karl-Josef Langen[2,5] · Christoph Kabbasch[3] · Norbert Galldiks[1,2,6,7,8]

Received: 5 March 2019 / Accepted: 30 May 2019 / Published online: 15 June 2019

Abstract

Background Following brain cancer treatment, the capacity of anatomical MRI to differentiate neoplastic tissue from treatment-related changes (e.g., pseudoprogression) is limited. This study compared apparent diffusion coefficients (ADC) obtained by diffusion-weighted MRI (DWI) with static and dynamic parameters of O-(2-[^{18}F]fluoroethyl)-L-tyrosine (FET) PET for the differentiation of treatment-related changes from tumour progression.

Patients and methods Forty-eight pretreated high-grade glioma patients with anatomical MRI findings suspicious for progression (median time elapsed since last treatment was 16 weeks) were investigated using DWI and dynamic FET PET. Maximum and mean tumour-to-brain ratios (TBR_{max}, TBR_{mean}) as well as dynamic parameters (time-to-peak and slope values) of FET uptake were calculated. For mean ADC calculation, regions-of-interest analyses were performed on ADC maps calculated from DWI coregistered with the contrast-enhanced MR image. Diagnoses were confirmed neuropathologically (21%) or clinicoradiologically. Diagnostic performance was evaluated using receiver-operating-characteristic analyses or Fisher's exact test for a combinational approach.

Results Ten of 48 patients had treatment-related changes (21%). The diagnostic performance of FET PET was significantly higher (threshold for both TBR_{max} and TBR_{mean}, 1.95; accuracy, 83%; AUC, 0.89 ± 0.05; $P < 0.001$) than that of ADC values (threshold ADC, 1.09×10^{-3} mm^2/s; accuracy, 69%; AUC, 0.73 ± 0.09; $P = 0.13$). The addition of static FET PET parameters to ADC values increased the latter's accuracy to 89%. The highest accuracy was achieved by combining static and dynamic FET PET parameters (93%). Moreover, in contrast to ADC values, TBRs <1.95 at suspected progression predicted a significantly longer survival ($P = 0.01$).

Conclusions Data suggest that static and dynamic FET PET provide valuable information concerning the differentiation of early treatment-related changes from tumour progression and outperform ADC measurement for this highly relevant clinical question.

Keywords Amino acid PET · Glioblastoma · Pseudoprogression · Tumour relapse · Diffusion-weighted imaging

Christoph Kabbasch and Norbert Galldiks contributed equally to this work.

This article is part of the Topical Collection on Neurology.

✉ Norbert Galldiks
n.galldiks@fz-juelich.de; norbert.galldiks@uk-koeln.de

[1] Department of Neurology, Faculty of Medicine and University Hospital Cologne, University of Cologne, Cologne, Germany

[2] Institute of Neuroscience and Medicine (INM-3, -4), Research Center Juelich, Juelich, Germany

[3] Department of Neuroradiology, Faculty of Medicine and University Hospital Cologne, University of Cologne, Cologne, Germany

[4] Department of Neurology, University Hospital Aachen, Aachen, Germany

[5] Department of Nuclear Medicine, University Hospital Aachen, Aachen, Germany

[6] Center of Integrated Oncology (CIO), Universities of Aachen, Bonn, Cologne, and Düsseldorf, Cologne, Germany

[7] Institute of Neuroscience and Medicine (INM-3), Research Center Juelich, Leo-Brandt-St. 5, 52425 Juelich, Germany

[8] Department of Neurology, University Hospital Cologne, Kerpener St. 62, 50937 Cologne, Germany

Introduction

Following local or systemic treatment options, the differentiation of tumour progression from treatment-related changes remains challenging despite its paramount clinical relevance. Here, standard contrast-enhanced MRI provides low specificity only [1–5]. Misjudging treatment-related changes as tumour progression may lead to a premature discontinuation of an effective treatment with a potentially negative impact on survival and an overestimation of the efficacy of the subsequent treatment [6]. The latter may also generate misleading results in studies evaluating salvage therapies [7].

Contrast-enhanced MRI is the method of choice for evaluating patients with primary brain tumours including gliomas and meningiomas as well as for secondary brain tumours such as brain metastases. This technique is widely available and provides an excellent spatial resolution, but its specificity is low, resulting in clinically important diagnostic challenges [2–5]. MRI signal changes (e.g., newly diagnosed contrast-enhancing lesions or an increase of the extent of contrast enhancement, signal alterations on T2/FLAIR sequences) may be related to ischemia, infection or neuroinflammation, demyelination, or treatment-related effects, i.e., reactive changes early after neurosurgery, radiotherapy, chemoradiation, systemic drug treatment including immunotherapy. All these changes can be difficult to distinguish from "true" tumour progression.

To overcome the limitations of conventional MRI, several efforts in the field of neuroimaging have been undertaken. For example, apparent diffusion coefficients (ADC) calculated from diffusion-weighted MRI (DWI) have been used to distinguish tumour progression from treatment-related changes [8–14]. In general, higher ADC values are consistent with treatment-related changes, most likely representing posttherapeutic extracellular edema, whereas lower ADC values are suspicious for neoplastic tissue [9, 13, 15–17]. A visual assessment of DWI hyperintensity associated with low ADC values may indicate active tumour tissue [15]. However, the results derived from the existing body of literature remain controversial. Several studies suggest that ADC values may be helpful for the differentiation between treatment-related changes and tumour progression [8, 13, 17, 18], whereas other studies reported a relatively poor diagnostic performance [9–12, 16, 19]. Furthermore, various DWI methods have been used and a considerable variability of optimal thresholds has been reported [8–13, 16, 17].

In recent years, PET using radiolabeled amino acids has become a valuable diagnostic tool for various indications in patients with brain tumours (e.g., delineation of tumour extent, assessment of treatment response, prognostication in patients with newly diagnosed gliomas). In particular, the high diagnostic value of amino acid PET compared to anatomical MRI for the differentiation of tumour progression from treatment-related changes has been reported in patients with glioma, meningioma and brain metastasis [1, 20–23]. Moreover, the Response Assessment in Neuro-Oncology (RANO) working group has recently recommended the use of amino acid PET imaging for glioma management in addition to conventional MRI at every disease stage [24, 25].

Regarding the clinically essential assessment of treatment-related changes, the number of available studies that directly compare two advanced imaging modalities remain scarce [26]. Thus, we here compared the diagnostic performance of ADC values with static and dynamic FET PET parameters for the differentiation of tumour progression from treatment-related changes in patients with malignant glioma.

Patients and methods

Patients and treatment

We retrospectively assessed data from 48 patients (mean age, 50 ± 15 years; age range, 20–83 years; 19 women and 29 men) with neuropathologically confirmed malignant glioma (Table 1). The data had been acquired from 2012 to 2018. All patients exhibited a newly diagnosed contrast-enhancing lesion or an enlargement of a preexisting contrast-enhancing lesion of more than 25% according to the RANO criteria on standard MRI using a gadolinium-based contrast agent after completion of the neurooncological treatment [6]. The mean time between completion of the last treatment regimen and suggested tumour progression was 30 ± 38 weeks (median time, 16 weeks; range, 2–222 weeks). In the majority of patients (77%), a glioblastoma was diagnosed, and treatment was initiated according to the EORTC 26981/22981 trial [27]. Further details on the patients' characteristics and pretreatment are listed in Table 1. To differentiate between treatment-related changes and tumour progression all patients were additionally investigated using FET PET. The mean time between MRI suspicious for tumour progression and FET PET imaging was 16 ± 15 days. DWI was obtained at the time point of suspected tumour progression. The local ethics committees approved the retrospective analysis of the data. There was no conflict with the Declaration of Helsinki. Before PET imaging, all subjects had given written informed consent for the PET investigation and the use of the data for scientific purposes.

Diagnosis of tumour progression or treatment-related changes

The diagnosis of tumour progression or treatment-related changes was based on the criteria defined by Young and colleagues [28]. Lesions on the initial MRI scan that worsened after completion of the neurooncological treatment were

Table 1 Demographic and clinical data

Patient number	Age (years)	Sex	Diagnosis	MGMT promoter methylation	EoR	First line therapy	Second line therapy	Time between therapy and suspicious MRI (weeks)
1	45	M	GBM, IDH-wt	Unmethylated	CR	TMZ-RCx	–	10
2	34	M	GBM, IDH-mut	Methylated	PR	TMZ-RCx	–	7
3	66	F	GBM, IDH-wt	Unmethylated	B	TMZ-RCx	–	12
4	67	M	GBM, IDH-wt	Methylated	B	TMZ-RCx	–	11
5	49	F	GBM, IDH-wt	Unmethylated	PR	RCx	–	6
6	52	M	GBM, IDH-wt	Unmethylated	CR	RCx	–	7
7	51	M	GBM, IDH-wt	Methylated	CR	RCx	–	6
8	61	M	GBM, IDH-wt	Unmethylated	B	TMZ-RCx	–	9
9	57	M	GBM, IDH-wt	Unmethylated	B	RCx	–	4
10	77	M	GBM, IDH-wt	Methylated	B	TMZ-RCx	–	7
11	52	F	GBM, IDH-wt	Unmethylated	PR	TMZ-RCx	–	19
12	63	M	GBM, IDH-wt	Methylated	CR	TMZ-RCx	–	40
13	24	M	GBM, IDH-wt	Methylated	CR	TMZ-RCx	–	39
14	20	F	GBM, IDH-wt	Methylated	B	TMZ-RCx	–	78
15	46	F	AO, IDH-mut and 1p/19q co-deleted	Methylated	B	TMZ	–	221
16	40	M	GBM, IDH-wt	Unmethylated	B	TMZ-RCx	–	14
17	47	M	GBM, IDH-wt	Unmethylated	CR	RCx	–	6
18	50	F	GBM, IDH-wt	Unmethylated	CR	TMZ-RCx	BT	60
19	33	F	AO, IDH-mut and 1p/19q co-deleted	Methylated	CR	RT; adjuvant TMZ	–	24
20	50	M	GBM, IDH-wt	Unmethylated	CR	RCx	–	2
21	26	M	GBM, IDH-mut	Methylated	B	TMZ-RCx	CCNU	38
22	54	F	GBM, IDH-wt	Unmethylated	B	TMZ-RCx	–	11
23	26	F	GBM, IDH-wt	Methylated	B	TMZ-RCx	–	6
24	33	F	GBM, IDH-mut	Methylated	PR	TMZ-RCx	–	43
25	47	M	GBM, IDH-wt	Methylated	B	TMZ-RCx	–	62
26	51	F	GBM, IDH-wt	Unmethylated	CR	TMZ-RCx	–	16
27	29	F	GBM, IDH-wt	Methylated	PR	TMZ-RCx	BT; CCNU	72
28	54	M	GBM, IDH-wt	Unmethylated	PR	TMZ-RCx	OP and TMZ	28
29	44	M	GBM, IDH-wt	Unmethylated	PR	TMZ-RCx	–	27
30	75	M	GBM, IDH-wt	Unmethylated	B	BT; adjuvant TMZ	–	41
31	55	M	GBM, IDH-wt	unmethylated	PR	TMZ-RCx	–	25
32	53	M	GBM, IDH-wt	methylated	PR	TMZ-RCx	–	25
33	56	F	GBM, IDH-wt	Unmethylated	CR	TMZ-RCx	–	25
34	57	F	AO, IDH-mut and 1p/19q co-deleted	Methylated	B	RT; adjuvant TMZ	–	38
35	45	F	secondary GBM, IDH-wt	Unmethylated	CR	TMZ	OP; TMZ-RCx	14
36	61	M	AA, IDH-mut	Methylated	B	RT; adjuvant TMZ	–	4
37	48	F	GBM, IDH-wt	Unmethylated	B	TMZ-RCx	–	9
38	33	M	GBM, IDH-wt	Methylated	PR	TMZ-RCx	TMZ-RCx	10
39	73	M	AA, IDH-wt	Unmethylated	B	TMZ-RCx	–	10
40	62	M	GBM, IDH-wt	Unmethylated	PR	RCx	–	12
41	47	M	GBM, IDH-wt	Unmethylated	PR	TMZ-RCx	–	16
42	52	M	AO, IDH-mut and 1p/19q co-deleted	Methylated	CR	RT; adjuvant PC	–	11
43	74	F	GBM, IDH-wt	Methylated	CR	TMZ-RCx	PC	44
44	83	M	GBM, IDH-wt	Unmethylated	CR	RT	–	25
45	43	M	AA, IDH-wt	Methylated	CR	TMZ-RCx	Px; TMZ	38

Table 1 (continued)

Patient number	Age (years)	Sex	Diagnosis	MGMT promoter methylation	EoR	First line therapy	Second line therapy	Time between therapy and suspicious MRI (weeks)
46	67	F	AO, IDH-mut and 1p/19q co-deleted	Methylated	B	BT; TMZ-RCx	–	132
47	44	M	GBM, IDH-mut	Methylated	B	TMZ-RCx	–	53
48	20	F	Diffuse midline glioma, H3-K27 M-mut	n.a.	PR	TMZ-RCx	–	4

AA anaplastic astrocytoma, *AO* anaplastic oligodendroglioma, *B* stereotactic biopsy, *BT* brachytherapy with iodine-125, *CCNU* lomustine, *CR* complete resection, *EoR* extent of resection, *F* female, *GBM* glioblastoma, *IDH* isocitrate dehydrogenase, *M* male, *mut* mutant, *n.a.* not available, *OP* tumor resection, *PC* adjuvant procarbazine and CCNU chemotherapy, *PR* partial resection, *Px* proton beam therapy, *RCx* radiotherapy with concomitant temozolomide chemotherapy, *RT* radiotherapy, *TMZ* adjuvant temozolomide chemotherapy, *TMZ-RCx* radiotherapy with concomitant and adjuvant temozolomide chemotherapy, *wt* wildtype

categorized as either tumour progression or treatment-related changes based on neuropathological analysis after repeated biopsy or resection when available (10 patients; 21%). Treatment-related changes were characterized by prominent necrosis with no or only minimal identifiable tumour remnants. The presence of viable tumour tissue confirmed tumour progression.

If a neuropathological diagnosis was unavailable (38 patients; 79%), tumour progression or treatment-related changes were confirmed clinicoradiologically. For this, clinical evaluation and contrast-enhanced MRI were performed every 2–3 months. Tumour progression was considered if imaging or clinical worsening prompted a change in treatment. Treatment-related changes were assumed if no change in anticancer treatment (e.g., change to another alkylating chemotherapy, re-resection, re-radiation, etc.) was required for at least 6 months. This definition allowed a continued mild increase of enhancing lesions, as compared to the usual decrease or stabilization, as long as no anticancer treatment change occurred during this period [28].

Conventional MR imaging

At the time point of suspected tumour progression, all patients had a routine MRI scan using a 1.5 T or 3.0 T MRI scanner (1.5 T Intera or 3.0 T Ingenia, Philips Healthcare, Best, The Netherlands) with a standard head coil before and after administration of a gadolinium-based contrast agent (T1, T2, and FLAIR).

Diffusion-weighted MRI

DWI was carried out on a 1.5 T or 3.0 T MRI system (1.5 T Intera or 3.0 T Ingenia, Philips Healthcare, Best, The Netherlands) with b-values of 0 s/mm^2 and 1000 s/mm^2. Sequence details for the 1.5 T system are: 30 slices, slice thickness of 5 mm, field-of-view of 23 cm, acquired matrix size of 112 × 90 pixels, and a reconstructed matrix size of 228 × 228 pixels. The sequence applied at 3.0 T consisted of 30 slices, slice thickness of 5 mm, field-of-view of 25 cm, acquired matrix size of 168 × 111 pixels, and a reconstructed matrix size of 320 × 320 pixels. ADC maps were calculated using the vendor-provided software. For data evaluation, the Picture Archiving and Communication System (Impax ee, Agfa Healthcare, Bonn, Germany) was used. Regions-of-interest (ROI) analyses were performed by three blinded and independent readers with more than 5 years of experience in the interpretation of MR imaging (T.L., C.K., J.B.). Two-dimensional ROI analyses were performed on T1-weighted post-contrast images corresponding to the entire measurable enhancing portion of the lesion on the section with maximum lesion extent suspected for tumour progression, excluding areas of necrosis or cysts. Subsequently, ROIs were transferred to the coregistered ADC maps for the calculation of mean ADC values.

FET PET imaging

As described previously, the amino acid FET was produced via nucleophilic ^{18}F-fluorination with a radiochemical purity of greater than 98%, specific radioactivity greater than 200 GBq/μmol, and a radiochemical yield of about 60% [29]. According to national and international guidelines for brain tumour imaging using labeled amino acid analogues [25, 30], all patients fasted for at least 4 h before the PET measurements. All patients underwent a dynamic PET scan from 0 to 50 min post-injection of 3 MBq of FET per kg of body weight. PET imaging was performed either on an ECAT Exact HR+ PET scanner ($n = 37$ patients) in 3-dimensional mode (Siemens, Erlangen, Germany) (axial field-of-view, 15.5 cm) or simultaneously with 3 T MR imaging using a BrainPET insert ($n = 11$ patients) (Siemens, Erlangen, Germany). The BrainPET is a compact cylinder that fits into the bore of the Magnetom Trio MR scanner (axial field of view, 19.2 cm) [31].

Iterative reconstruction parameters were 16 subsets, 6 iterations using the OSEM algorithm for ECAT HR+ PET scanner and two subsets, 32 iterations using the OP-OSEM algorithm for the BrainPET. Data were corrected for random, scattered coincidences, dead time, and motion for both systems. Attenuation correction for the ECAT HR+ PET scan was based on a transmission scan, and for the BrainPET scan on a template-based approach [31]. The reconstructed dynamic data set consisted of 16 time frames (5 × 1 min; 5 × 3 min; 6 × 5 min) for both scanners.

To optimize comparability of the results related to the influence of the two different PET scanners, reconstruction parameters, and post-processing steps, a 2.5-mm 3D Gaussian filter was applied to the BrainPET data prior to further processing, resulting in an image resolution of approximately 4 mm (image resolution of the ECAT HR+ PET scanner, approximately 6 mm). In phantom experiments using spheres of different sizes to simulate lesions, this filter kernel demonstrated the best comparability between PET data obtained from the ECAT HR+ PET and the BrainPET scanner [32].

FET PET data analysis

FET PET data analysis was performed as described previously [33]. In brief, for the evaluation of FET data summed PET images over the period of 20–40 min post-injection were used. Mean amino acid uptake in the tumour was determined by a 2-dimensional auto-contouring process using a tumour-to-brain ratio (TBR) of 1.6 as described previously [34, 35]. For the calculation of the maximal amino acid uptake, a circular ROI with a diameter of 1.6 cm was centered on the maximal tumour uptake [33]. Maximum and mean TBRs (TBR_{max}, TBR_{mean}) were calculated by dividing the mean SUV of the tumour ROIs by the mean SUV of healthy brain tissue.

As described previously [33], time-activity curves (TACs) of FET uptake in the tumour were generated by the application of a spherical volume-of-interest (VOI) with a volume of 2 mL centered on maximal tumour uptake to the entire dynamic dataset. A reference TAC was generated by placing a reference ROI in the unaffected brain tissue (as described above). For TAC evaluation, the time-to-peak (TTP; time in minutes from the beginning of the dynamic acquisition up to the maximum SUV of the lesion) was determined. In cases with constantly increasing FET uptake without identifiable peak uptake, we have defined the end of the dynamic PET acquisition as TTP. Furthermore, the slope of the TAC in the late phase of FET uptake was assessed by fitting a linear regression line to the late phase of the curve (20–50 min post-injection). The slope was expressed as the change of the SUV per hour. This allows for a more objective evaluation of kinetic data compared to an assignment of TACs to earlier reported patterns of FET uptake during dynamic acquisition [33].

Definition of survival times

The post-index survival was defined as the time between the MRI, which caused the suspicion of tumour progression, and death. The median follow-up of all patients was 8 months (range, 1–75 months).

Neuropathological tumour classification and analysis of molecular markers

All tumours were neuropathologically classified as gliomas according to the World Health Organization (WHO) Classification for tumours of the Central Nervous System of 2016 [36]. For the isocitrate dehydrogenase (IDH) mutation status, the presence of IDH1R132H protein expression was evaluated by immunohistochemistry. If immunostaining was negative, IDH was directly sequenced. The 1p/19q co-deletion status was analyzed by PCR-based microsatellite analysis. O^6-methylguanine-DNA-methyltransferase (MGMT) promoter methylation analysis was executed after DNA extraction from samples containing vital glioblastoma tissue with a histologically estimated tumour cell content of 80% or more. MGMT promoter methylation was assessed using a methylation-specific PCR as described elsewhere [37].

Statistical analyses

Descriptive statistics are provided as mean and standard deviation and/or median and range. The Student t-test for independent samples was used to compare two different groups. The Mann-Whitney rank-sum test was used when variables were not normally distributed. The diagnostic performance of FET uptake, as determined by TBR_{max} and TBR_{mean}, TTP, slope, and ADC values from DWI to identify treatment-related changes was assessed by receiver operating characteristic (ROC) curve analyses using neuropathological confirmation or clinical course as the reference. Decision cut-off was considered optimal when the product of paired values for sensitivity and specificity reached its maximum. Besides, the area under the ROC curve (AUC), its standard error, and level of significance were determined as a measure of the diagnostic quality of the test. The diagnostic performance of TBRs in combination with the corresponding ADC, TTP, or slope values was evaluated by the Fisher exact test for 2 × 2 contingency tables. Survival analyses were performed using the log-rank test. For the visual assessment of the ADC maps, Cohen's κ was used to estimate the interrater reliability among the rating neuroradiologists (T.L., C.K., J.B.). κ-values between 0 and 0.20 were considered to indicate a positive but slight correlation, between 0.21 and 0.40 a moderate correlation, between 0.41 and 0.60 a good correlation, between 0.61 and 0.80 a very good correlation, and greater than 0.80 an excellent correlation. *P* values of 0.05 or less were considered

significant. Statistical analyses were performed using SPSS statistics (Release 25.0, SPSS Inc., Chicago, IL, USA) and Prism GraphPad (Release 7.00c, GraphPad Software Inc., La Jolla, CA, USA).

Results

Diagnoses

Thirty-eight of the 48 patients had tumour progression (79%) and the remaining ten patients had treatment-related changes (21%) (Table 2). Neuropathologically, tumour progression with viable tumour tissue was confirmed in nine patients, and one patient had treatment-related changes without viable tumour cells (Fig. 1). Clinicoradiologically, tumour progression was confirmed in 29 patients, whereas in nine patients the diagnosis of treatment-related changes was confirmed by a stable clinical course of at least 6 months or more, with stable or regressive MRI findings without any treatment change (Fig. 2). No significant group differences (treatment-related changes vs. tumour progression) were observed regarding age (47 ± 18 vs. 51 ± 14 years; $P = 0.57$), extent of resection (complete vs. partial resection or stereotactic biopsy; $P = 0.82$), IDH mutation (IDH wildtype vs. IDH mutated; $P = 0.57$), and MGMT promoter methylation (methylated vs. non-methylated; $P = 0.29$).

Static FET PET parameters

TBR_{max} and TBR_{mean} of FET uptake (Table 2) were significantly lower in patients with treatment-related changes than in patients with tumour progression (TBR_{max}, 1.7 ± 0.2 vs. 2.6 ± 0.7, $P < 0.001$; TBR_{mean}, 1.7 ± 0.2 vs. 2.1 ± 0.3, $P < 0.001$). The ROC analysis revealed that the optimal cut-off value of both TBR_{max} and TBR_{mean} for the identification of treatment-related changes was 1.95 (sensitivity, 100%; specificity, 79%; accuracy, 83%; AUC 0.89 ± 0.05; $P < 0.001$) (Table 3).

Dynamic FET PET parameters

The ROC analysis revealed an optimal TTP cut-off value of 32.5 min for the differentiation of treatment-related changes from tumour progression (accuracy, 72%; sensitivity, 80%; specificity, 69%; AUC 0.79 ± 0.07; $P < 0.01$). For slope, the ROC analysis revealed for the optimal cut-off value of 0.32 SUV/h a slightly higher diagnostic accuracy of 74% (sensitivity, 70%; specificity, 75%; AUC 0.82 ± 0.06; $P = 0.02$) (Table 4).

Combined analysis of static and dynamic FET PET parameters

The highest diagnostic performance was obtained combining static FET PET parameters and slope. In particular, a TBR_{max} or TBR_{mean} value <1.95 in combination with a slope > 0.32 SUV/h revealed a diagnostic accuracy of 93% (sensitivity, 78%; specificity, 97%; $P < 0.001$). A TBR_{mean} or TBR_{max} value <1.95 in combination with a TTP > 32.5 min revealed a slightly lower diagnostic accuracy of 90% (sensitivity, 89%; specificity, 91%; $P < 0.001$). Further details of the diagnostic performance of combinations are listed in Table 4.

ADC

There was good interrater reliability for visual assessment of ADC maps with a mean κ value of 0.71 ± 0.10 (range, 0.65–0.83). The identification of treatment-related changes by visual assessment alone was not statistically significant (sensitivity, 70%; specificity, 66%; accuracy, 67%; $P = 0.07$) (Table 3).

The averaged ADC (Table 2) was significantly higher in patients with treatment-related changes than in patients with tumour progression ($1.23 \pm 0.4 \times 10^{-3}$ mm^2/s vs. $0.96 \pm 0.4 \times 10^{-3}$ mm^2/s; $P = 0.023$). The ROC analysis showed that the optimal ADC cut-off value for identifying treatment-related changes was $>1.09 \times 10^{-3}$ mm^2/s (sensitivity, 60%; specificity, 71%; accuracy, 69%; AUC, 0.73 ± 0.09; $P = 0.13$) (Table 3). The combination of ADC > 1.09 and static FET PET parameters (TBR_{max} or $TBR_{mean} < 1.95$) increased the diagnostic accuracy (sensitivity, 67%; specificity, 94%; accuracy, 89%; $P < 0.001$) (Table 3).

Significant ADC differences related to the IDH mutational status could not be observed (averaged ADC in IDH-wildtype gliomas of $0.98 \pm 0.4 \times 10^{-3}$ mm^2/s compared to the averaged ADC in IDH-mutated gliomas of $1.1 \pm 0.5 \times 10^{-3}$ mm^2/s; $P = 0.33$).

Survival

The post-index survival in patients with treatment-related changes was significantly longer than in patients with tumour progression (not reached vs. 8 months; $P = 0.002$). Both TBR_{max} and TBR_{mean} below the threshold of 1.95 values predicted a significantly longer post-index survival (not reached vs. 8 months; $P = 0.01$). In contrast, an ADC value above the threshold of 1.09×10^{-3} mm^2/s was unable to predict a longer post-index survival ($P = 0.11$).

Discussion

The main finding of the present study is that FET PET-derived imaging parameters provide valuable clinical information for

Table 2 Imaging results in relation to diagnoses and survival

Patient number	TBR_{max}	TBR_{mean}	TTP (minutes)	Slope (SUV/h)	ADC value ($\times 10^{-3}$ mm^2/s)	Confirmation of diagnosis	Diagnosis	Time between suspicious MRI and death (months)
1	1.8	1.8	30	0.18	0.89	clin-rad	Treatment-related changes	12
2	1.9	1.9	35	0.97	1.09	clin-rad	Treatment-related changes	69[a]
3	3.2	2.3	20	−0.10	1.15	clin-rad	TP	6
4	2.4 [b]	2.1 [b]	25	−0.22	0.65	clin-rad	Treatment-related changes	23[a]
5	1.9	1.8	17	0.10	1.09	clin-rad	TP	8
6	2.5 [c]	1.9 [c]	30	0.23	1.12	clin-rad	TP	11
7	3.8	2.7	8	−3.68	0.98	neuropathol (R)	TP	22[a]
8	2.4 [b]	1.9 [b]	25	0.12	0.82	clin-rad	TP	1
9	3.1	2.2	17	−0.80	0.79	clin-rad	TP	4
10	2.9	2.1	17	−0.44	0.60	clin-rad	TP	1
11	2.4	2.0	14	−0.77	0.52	clin-rad	TP	14
12	3.5	3.1	35	0.72	0.57	clin-rad	TP	8
13	2.2	2.2	11	−0.04	1.05	neuropathol (B)	TP	9[a]
14	3.3	2.2	25	−0.69	0.52	clin-rad	TP	7
15	1.8	1.8	35	−0.31	0.91	neuropathol (B)	TP	13[a]
16	3.0	2.3	40	0.29	0.90	clin-rad	TP	5
17	2.4	2.0	20	−0.71	0.75	clin-rad	TP	6
18	2.0	2.0	40	1.02	0.83	neuropathol (B)	TP	6
19	1.7	1.7	35	1.04	1.25	clin-rad	Treatment-related changes	20[a]
20	2.0	2.0	30	−0.50	0.58	neuropathol (R)	TP	11
21	1.9 [c]	1.9 [c]	2	0.38	0.91	clin-rad	TP	2
22	3.3	2.2	25	0.31	0.88	clin-rad	TP	8
23	1.8	1.8	35	0.75	1.59	clin-rad	Treatment-related changes	24[a]
24	2.6	2.1	14	−0.09	0.63	clin-rad	TP	11
25	2.5	2.2	25	−0.24	1.06	clin-rad	TP	4
26	1.8	1.8	35	0.51	1.39	clin-rad	Treatment-related changes	7[a]
27	2.5	2.2	35	2.12	0.39	neuropathol (R)	TP	7
28	4.0	2.5	14	−0.48	0.93	clin-rad	TP	7[a]
29	2.3	2.1	30	−0.01	1.13	clin-rad	TP	16
30	2.9	2.4	25	−0.34	0.93	clin-rad	TP	6
31	2.0	2.0	20	−0.42	1.13	clin-rad	TP	7
32	3.8	2.6	20	−1.24	1.32	clin-rad	TP	6
33	1.7	1.7	14	−0.16	0.92	clin-rad	TP	9
34	2.6	2.2	35	1.62	1.17	clin-rad	TP	8[a]
35	2.1	2.1	45	0.06	0.93	clin-rad	TP	5
36	2.9	2.2	20	−1.06	1.70	clin-rad	TP	36[a]
37	3.3	2.3	40	0.81	1.13	neuropathol (R)	TP	27
38	2.2	2.1	40	0.47	1.03	clin-rad	TP	35
39	1.9	1.9	45	0.32	1.25	clin-rad	Treatment-related changes	19
40	1.8	1.8	35	0.24	0.74	clin-rad	TP	5
41	1.8	1.8	35	0.58	1.33	neuropathol (R)	TP	7[a]
42	1.7	1.7	35	0.81	2.10	clin-rad	Treatment-related changes	7[a]
43	1.7	1.7	n.a.	n.a.	0.83	clin-rad	TP	7[a]

Table 2 (continued)

Patient number	TBR_{max}	TBR_{mean}	TTP (minutes)	Slope (SUV/h)	ADC value ($\times 10^{-3}$ mm^2/s)	Confirmation of diagnosis	Diagnosis	Time between suspicious MRI and death (months)
44	2.4	2.2	14	−0.93	1.20	clin-rad	TP	1[a]
45	1.0	1.0	n.a.	n.a.	2.38	neuropathol (B)	TP	3[a]
46	1.3	1.3	40	1.19	0.96	neuropathol (B)	Treatment-related changes	75[a]
47	2.6	2	30	0.69	0.75	clin-rad	TP	21[a]
48	1.7	1.7	35	0.09	1.13	clin-rad	Treatment-related changes	7[a]

ADC mean apparent diffusion coefficient obtained from DWI, *(B)* neuropathological diagnosis confirmed by stereotactic biopsy, *clin-rad* clinicoradiologically, *n.a.* not available, *neuropathol* neuropathologically confirmed diagnosis by biopsy or resection, *(R)* neuropathological diagnosis confirmed by resection, *SUV* standardized uptake value, TBR_{mean} mean tumor-to-brain ratio of FET PET uptake, TBR_{max} maximum tumor-to-brain ratio of FET PET uptake, *TTP* time-to-peak, *TP* tumor progression

[a] Censored patients

[b] Decrease of TBRs compared to baseline FET PET

[c] FET uptake in new lesions compared to baseline FET PET

the identification of treatment-related changes in patients with malignant glioma. Importantly, the combination of static and dynamic FET PET parameters further increases the diagnostic accuracy. Although ADC maps derived from DWI were also able to identify treatment-related changes, the diagnostic performance of FET PET parameters was superior, indicating that FET PET is the diagnostic imaging modality of choice for this important clinical question. Moreover, the addition of FET PET parameters to ADC values increased the latter's weak diagnostic performance and allowed a meaningful identification of treatment-related changes.

The high diagnostic accuracy of FET PET in differentiating between tumour progression and treatment-related changes in glioma patients has been shown repeatedly [1, 18, 19, 33, 38–41]. In the present study, the high diagnostic accuracy (83%) of the static FET PET parameters TBR_{max} and TBR_{mean} using a cut-off value of 1.95 was in the range of previously reported results [1, 19, 33, 38, 41, 42].

The diagnostic accuracy of dynamic FET PET parameters was lower than that of static FET PET parameters, which is in line with previous reported results [19]. Notwithstanding the above, the combination of static and dynamic FET PET parameters showed a further increase in diagnostic performance. Both TBR_{mean} and TBR_{max} achieved a high diagnostic accuracy of 93% in combination with dynamic FET PET parameters, similar to earlier reported results in patients with glioma and brain metastases [21, 33].

The higher diagnostic performance of FET PET compared to ADC values in differentiating treatment-related changes from tumour progression is in accordance with other multimodal imaging studies using FET PET [18, 19]. On the other hand, the diagnostic performance of mean ADC values without the combination with information derived from other imaging modalities was not convincing. Similarly, previous studies reported either a sensitivity or specificity of mean ADC values of 50% or less, and, consistent with our data, only the combination of ADC with parameters derived from FET PET and/or other MRI techniques increased the diagnostic performance [18, 19].

The higher diagnostic accuracy of static and dynamic FET PET is most probably related to various factors. The higher specificity of FET for neoplastic tissue is related to the overexpression of amino acid transporters (subtypes LAT1 and LAT2) [43]. In contrast, in subacute treatment-related local tissue changes which comprises inflammation [44], amino acid transporters are usually not overexpressed. However, although this is much less common, it should be kept in mind that usually mild, but increased amino acid tracer uptake may also occur in infectious (e.g., brain abscess) or inflammatory processes (e.g., acute multiple sclerosis) [45]. Regarding perfusion, major spatial differences have been observed between the extent of FET uptake and relative cerebral blood volume as assessed by perfusion MRI, indicating that the regional tumor perfusion influences the FET uptake only insignificantly [46–48]. Furthermore, another study suggested that the late phase of TACs is not significantly influenced by relative cerebral blood flow [49]. Extracellular factors such as vasogenic edema may also affect the FET uptake only insignificantly, even if dexamethasone is administered [50].

Regarding the diagnostic performance of various other ADC parameters (e.g., maximum and median ADC, ADC percentiles, kurtosis, skewness, entropy) used for the differentiation of treatment-related changes from tumour progression, the literature suggests a considerable variability of diagnostic performance (range of sensitivity, 50–100%; range of specificity, 43–100%) [8, 13, 16–19, 51]. Moreover, a few studies reported the inability of ADC measurements to significantly differentiate between treatment-related changes and tumour

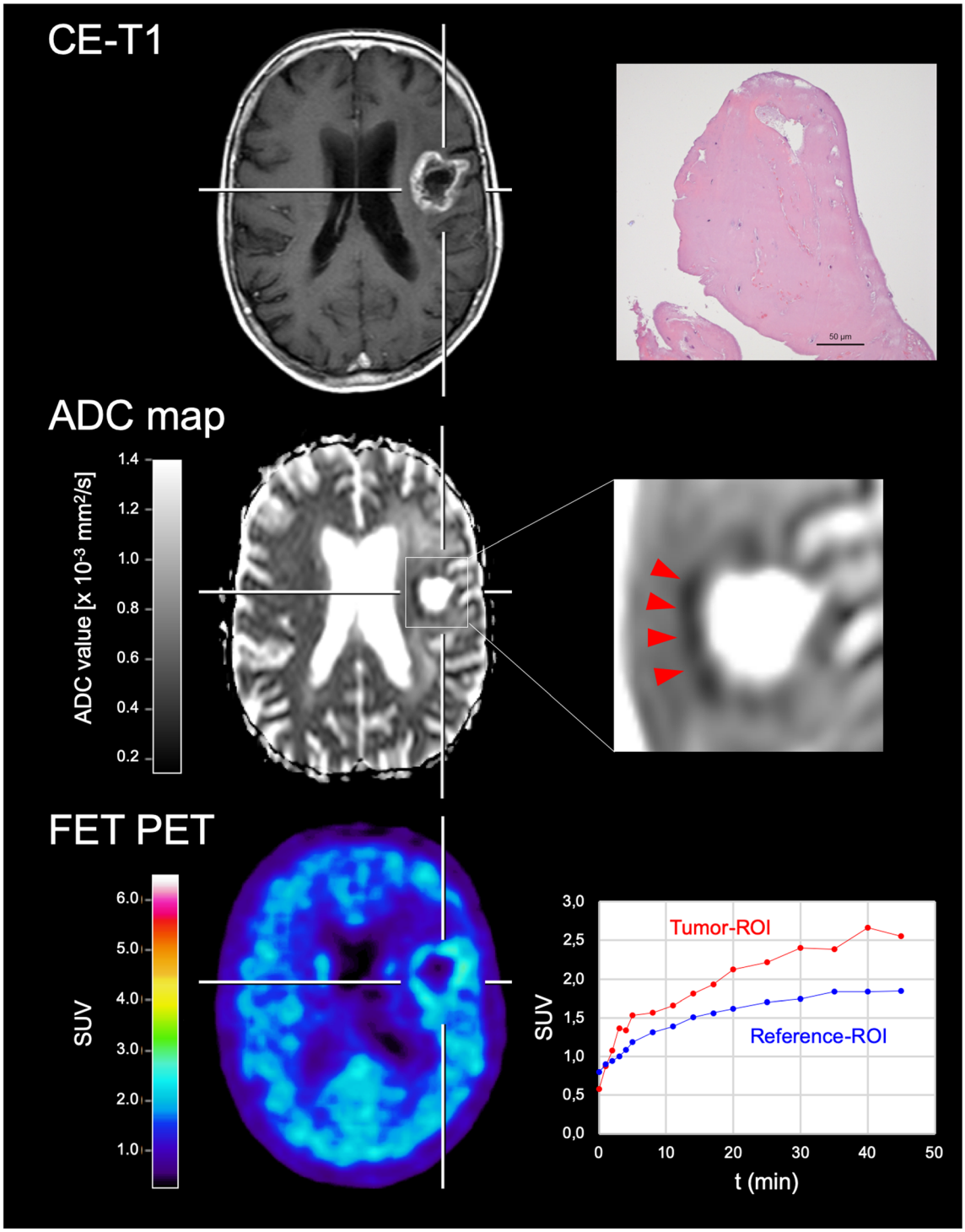

Fig. 1 Contrast-enhanced MRI, ADC map obtained from DWI, and FET PET of a 69-year old female patient (#46) with anaplastic oligodendroglioma. Twenty-nine months after fractionated external beam radiotherapy, brachytherapy, and adjuvant temozolomide chemotherapy, contrast-enhanced MRI suggested tumour progression. In spatial correspondence to the contrast enhancement, the ADC map revealed a substantial decrease of diffusivity in the area of contrast enhancement (arrowheads on the enlarged image; ADC below 0.5×10^{-3} mm^2/s), suggesting tumour progression. In contrast, FET PET showed no increased metabolic activity and a steadily increasing time-activity curve, indicating treatment-related changes. Histological findings obtained following stereotactic biopsy were consistent with radiation necrosis (hematoxylin and eosin staining, original magnification ×200; scale bar, 50 µm). For a follow-up time of 6 years, the patient was in a stable clinical condition. Parts of Fig. 1 have been published in an earlier study of our group [33]

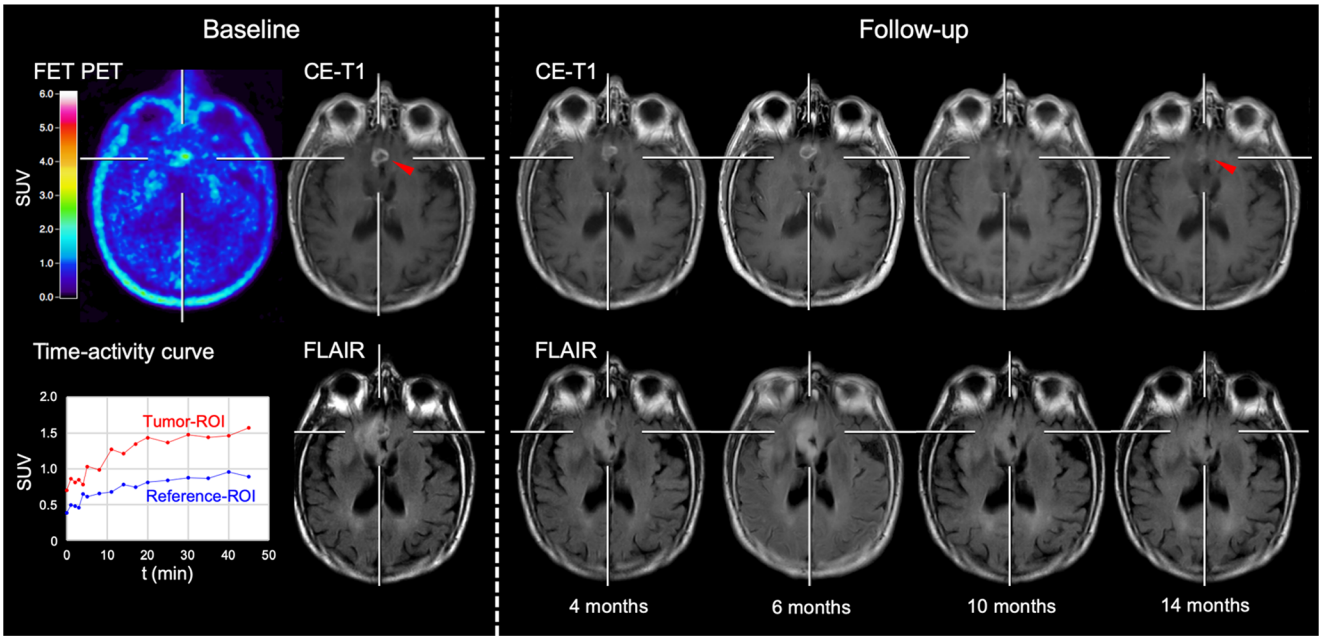

Fig. 2 Contrast-enhanced MRI, FLAIR MRI, and FET PET of a 73-year old male patient (#39) with a newly diagnosed anaplastic astrocytoma (IDH wildtype, MGMT promoter not methylated). Ten weeks after completion of radiotherapy with concomitant temozolomide chemotherapy (baseline), contrast-enhanced MRI indicated tumour progression (*left arrow*). In contrast, FET PET showed no increased metabolic activity (TBR_{max}, 1.9; TBR_{mean}, 1.9) and a steadily increasing time-activity curve (TTP, 45 min; slope, 0.32 SUV/h), suggesting treatment-related changes. Without treatment change, the patient was followed for clinical and radiological signs of tumour progression. Serial follow-up MR imaging revealed a decrease of contrast enhancement over time. Fourteen months after completion of chemoradiation, the contrast-enhancing lesion vanished almost completely (*right arrow*) and the FLAIR hyperintensity decreased during follow-up

progression [11, 52], which is in line with our data. Other causes than increased cellularity in neoplastic tissue, e.g., ischemia, infection, inflammation, gliosis, necrosis, or vascular proliferation, may alter diffusion, leading to heterogeneous signal intensity, and thereby causing considerable variability of diagnostic performance of parameters obtained from DWI [2, 53, 54]. Additionally, ADC maps have a relatively poor spatial resolution and signal-to-noise ratio, and ADC values may show a significant variability depending on the utilized coils, vendors, field strengths, and sequence parameters used for MR imaging [55, 56]. On the other hand, the variance of the ADC values obtained from different MRI scanners is relatively low if comparable DWI sequences and postprocessing are used (as in the present study) [57]. Furthermore, ADC values may also be affected by the IDH mutation status. A recent study showed lower ADC values in IDH wildtype gliomas compared to IDH mutant gliomas [58]. However, the latter result could not be replicated in the present study.

Table 3 Diagnostic performance of static FET PET parameters, ADC metrics and combinations thereof

Performance measure	TBR_{max}	TBR_{mean}	Visual assessment of ADC maps	ADC	Combined analysis of FET PET parameters and ADC
Threshold for the identification of treatment-related changes	< 1.95	< 1.95	n.a.	> 1.09×10^{-3} m-m^2/s	TBR_{mean} or TBR_{max} < 1.95 and ADC > 1.09
Sensitivity (%)	100	100	70	60	67
Specificity (%)	79	79	66	71	94
Diagnostic accuracy (%)	83	83	67	69	89
Positive predictive value (%)	56	56	35	35	75
Negative predictive value (%)	100	100	89	87	92
AUC ± standard deviation	0.89 ± 0.05	0.89 ± 0.05	n.a.	0.73 ± 0.09	n.a.
P value	< 0.001	< 0.001	0.07	0.13	< 0.001

ADC mean apparent diffusion coefficient obtained from DWI, *AUC* area under curve from a receiver operating characteristic curve, *n.a.* not available, *TBR_{max}* maximum tumor-to-brain ratio of FET PET uptake, *TBR_{mean}* mean tumor-to-brain ratio of FET PET uptake

Table 4 Diagnostic performance of combined static and dynamic FET PET parameters

Performance measure	TTP	Slope	Combined analysis of static and dynamic FET PET parameters	
Threshold for the identification of treatment-related changes	> 32.5 min	> 0.32 SUV/h	TBR_{max} or TBR_{mean} < 1.95 and presence of a TTP > 32.5 min	TBR_{max} or TBR_{mean} < 1.95 and presence of a slope > 0.32 SUV/h
Sensitivity (%)	80	70	89	78
Specificity (%)	69	75	91	97
Diagnostic accuracy (%)	72	74	90	93
Positive predictive value (%)	42	44	73	88
Negative predictive value (%)	93	90	97	94
AUC ± standard deviation	0.79 ± 0.07	0.82 ± 0.06	n.a.	n.a.
P value	0.009	0.02	< 0.001	< 0.001

AUC area under curve from a receiver operating characteristic curve, *n.a.* not available, *SUV* standardized uptake value, TBR_{max} maximum tumor-to-brain ratio of FET PET uptake, TBR_{mean} mean tumor-to-brain ratio of FET PET uptake, *TTP* time-to-peak

Nevertheless, a few studies reported that ADC values differentiate treatment-related changes from tumour progression with high diagnostic accuracy. Especially two studies (from a single institution) in newly-diagnosed glioblastoma patients treated according to the EORTC 26981/22981 trial [27] reported an excellent diagnostic performance (range of sensitivity, 98–100%; specificity, 100%), which has not been replicated [13, 17]. The present study was based on a more practice-oriented patient population (e.g., various glioma entities with different WHO grades, with or without pretreatment) and a balanced distribution of IDH mutations in patients with treatment-related changes and tumour progression. Studies with similarly heterogeneous patient collectives showed a lower diagnostic performance of ADC similar to our results [16, 19].

Besides the retrospective design, one could argue that the present study has several limitations. It has to be noted that a neuropathological validation of imaging findings was not available for all lesions, and clinicoradiological criteria had to be used for the final diagnosis in the majority of lesions. On the other hand, due to a poor clinical condition or refusal of the patient a biopsy or surgery cannot always be performed. Furthermore, dynamic scanning is more laborious and time-consuming. It is still unclear whether the improvement of diagnostic performance of dynamic scanning justifies the additional costs. This issue needs to be further evaluated in prospective studies with more extensive patient cohorts.

In summary, static FET PET imaging parameters such as TBRs offer high diagnostic performance for the identification of treatment-related changes. The combination of static and dynamic FET PET parameters further increases its diagnostic accuracy. In clinical routine, FET PET should be preferred over ADC measurement for the differentiation of tumour progression from treatment-related changes.

Funding The Wilhelm-Sander Stiftung, Germany, supported this work.

Compliance with ethical standards

Conflict of interest The authors declare that they have no conflict of interest.

Ethical approval All procedures performed in studies involving human participants were in accordance with the ethical standards of the institutional and/or national research committee and with the 1964 Helsinki declaration and its later amendments or comparable ethical standards.

Informed consent Informed written consent was obtained from all individual participants included in the study.

References

1. Galldiks N, Dunkl V, Stoffels G, Hutterer M, Rapp M, Sabel M, et al. Diagnosis of pseudoprogression in patients with glioblastoma using O-(2-[18F]fluoroethyl)-L-tyrosine PET. Eur J Nucl Med Mol Imaging. 2015;42:685–95.
2. Langen KJ, Galldiks N, Hattingen E, Shah NJ. Advances in neuro-oncology imaging. Nat Rev Neurol. 2017;13:279–89.
3. Ahluwalia MS, Wen PY. Antiangiogenic therapy for patients with glioblastoma: current challenges in imaging and future directions. Expert Rev Anticancer Ther. 2011;11:653–6.
4. Dhermain FG, Hau P, Lanfermann H, Jacobs AH, van den Bent MJ. Advanced MRI and PET imaging for assessment of treatment response in patients with gliomas. Lancet Neurol. 2010;9:906–20.
5. Kumar AJ, Leeds NE, Fuller GN, Van Tassel P, Maor MH, Sawaya RE, et al. Malignant gliomas: MR imaging spectrum of radiation therapy- and chemotherapy-induced necrosis of the brain after treatment. Radiology. 2000;217:377–84.
6. Wen PY, Macdonald DR, Reardon DA, Cloughesy TF, Sorensen AG, Galanis E, et al. Updated response assessment criteria for high-grade gliomas: response assessment in neuro-oncology working group. J Clin Oncol. 2010;28:1963–72.
7. Reardon DA, Weller M. Pseudoprogression: fact or wishful thinking in neuro-oncology? Lancet Oncol. 2018;19:1561–3.
8. Lee WJ, Choi SH, Park CK, Yi KS, Kim TM, Lee SH, et al. Diffusion-weighted MR imaging for the differentiation of true progression from pseudoprogression following concomitant

radiotherapy with temozolomide in patients with newly diagnosed high-grade gliomas. Acad Radiol. 2012;19:1353–61.
9. Hein PA, Eskey CJ, Dunn JF, Hug EB. Diffusion-weighted imaging in the follow-up of treated high-grade gliomas: tumor recurrence versus radiation injury. AJNR Am J Neuroradiol. 2004;25:201–9.
10. Asao C, Korogi Y, Kitajima M, Hirai T, Baba Y, Makino K, et al. Diffusion-weighted imaging of radiation-induced brain injury for differentiation from tumor recurrence. AJNR Am J Neuroradiol. 2005;26:1455–60.
11. Chu HH, Choi SH, Ryoo I, Kim SC, Yeom JA, Shin H, et al. Differentiation of true progression from pseudoprogression in glioblastoma treated with radiation therapy and concomitant temozolomide: comparison study of standard and high-b-value diffusion-weighted imaging. Radiology. 2013;269:831–40.
12. Yoo RE, Choi SH, Kim TM, Lee SH, Park CK, Park SH, et al. Independent poor prognostic factors for true progression after radiation therapy and concomitant temozolomide in patients with glioblastoma: subependymal enhancement and low ADC value. AJNR Am J Neuroradiol. 2015;36:1846–52.
13. Kazda T, Bulik M, Pospisil P, Lakomy R, Smrcka M, Slampa P, et al. Advanced MRI increases the diagnostic accuracy of recurrent glioblastoma: single institution thresholds and validation of MR spectroscopy and diffusion weighted MR imaging. Neuroimage Clin. 2016;11:316–21.
14. Weller M, van den Bent M, Tonn JC, Stupp R, Preusser M, Cohen-Jonathan-Moyal E, et al. European Association for Neuro-Oncology (EANO) guideline on the diagnosis and treatment of adult astrocytic and oligodendroglial gliomas. Lancet Oncol. 2017;18:e315–e29.
15. Padhani AR, Liu G, Koh DM, Chenevert TL, Thoeny HC, Takahara T, et al. Diffusion-weighted magnetic resonance imaging as a cancer biomarker: consensus and recommendations. Neoplasia. 2009;11:102–25.
16. Prager AJ, Martinez N, Beal K, Omuro A, Zhang Z, Young RJ. Diffusion and perfusion MRI to differentiate treatment-related changes including pseudoprogression from recurrent tumors in high-grade gliomas with histopathologic evidence. AJNR Am J Neuroradiol. 2015;36:877–85.
17. Bulik M, Kazda T, Slampa P, Jancalek R. The diagnostic ability of follow-up imaging biomarkers after treatment of glioblastoma in the Temozolomide era: implications from proton MR spectroscopy and apparent diffusion coefficient mapping. Biomed Res Int. 2015;2015:641023.
18. Jena A, Taneja S, Gambhir A, Mishra AK, D'Souza MM, Verma SM, et al. Glioma recurrence versus radiation necrosis: single-session multiparametric approach using simultaneous O-(2-18F-Fluoroethyl)-L-tyrosine PET/MRI. Clin Nucl Med. 2016;41:e228–36.
19. Pyka T, Hiob D, Preibisch C, Gempt J, Wiestler B, Schlegel J, et al. Diagnosis of glioma recurrence using multiparametric dynamic 18F-fluoroethyl-tyrosine PET-MRI. Eur J Radiol. 2018;103:32–7.
20. Galldiks N, Law I, Pope WB, Arbizu J, Langen KJ. The use of amino acid PET and conventional MRI for monitoring of brain tumor therapy. Neuroimage Clin. 2017;13:386–94.
21. Ceccon G, Lohmann P, Stoffels G, Judov N, Filss CP, Rapp M, et al. Dynamic O-(2-18F-fluoroethyl)-L-tyrosine positron emission tomography differentiates brain metastasis recurrence from radiation injury after radiotherapy. Neuro-Oncology. 2017;19:281–8.
22. Galldiks N, Langen KJ, Albert NL, Chamberlain M, Soffietti R, Kim MM, et al. PET imaging in patients with brain metastasis-report of the RANO/PET group. Neuro-Oncology. 2019;21:585–95.
23. Galldiks N, Albert NL, Sommerauer M, Grosu AL, Ganswindt U, Law I, et al. PET imaging in patients with meningioma-report of the RANO/PET group. Neuro-Oncology. 2017;19:1576–87.
24. Albert NL, Weller M, Suchorska B, Galldiks N, Soffietti R, Kim MM, et al. Response assessment in neuro-oncology working group and European Association for Neuro-Oncology recommendations for the clinical use of PET imaging in gliomas. Neuro-Oncology. 2016;18:1199–208.
25. Law I, Albert NL, Arbizu J, Boellaard R, Drzezga A, Galldiks N, et al. Joint EANM/EANO/RANO practice guidelines/SNMMI procedure standards for imaging of gliomas using PET with radiolabelled amino acids and [(18)F]FDG: version 1.0. Eur J Nucl Med Mol Imaging. 2019;46:540–57.
26. Sogani SK, Jena A, Taneja S, Gambhir A, Mishra AK, D'Souza MM, et al. Potential for differentiation of glioma recurrence from radionecrosis using integrated (18)F-fluoroethyl-L-tyrosine (FET) positron emission tomography/magnetic resonance imaging: a prospective evaluation. Neurol India. 2017;65:293–301.
27. Stupp R, Mason WP, van den Bent MJ, Weller M, Fisher B, Taphoorn MJ, et al. Radiotherapy plus concomitant and adjuvant temozolomide for glioblastoma. N Engl J Med. 2005;352:987–96.
28. Young RJ, Gupta A, Shah AD, Graber JJ, Zhang Z, Shi W, et al. Potential utility of conventional MRI signs in diagnosing pseudoprogression in glioblastoma. Neurology. 2011;76:1918–24.
29. Hamacher K, Coenen HH. Efficient routine production of the 18F-labelled amino acid O-2-18F fluoroethyl-L-tyrosine. Appl Radiat Isot. 2002;57:853–6.
30. Langen KJ, Bartenstein P, Boecker H, Brust P, Coenen HH, Drzezga A, et al. German guidelines for brain tumour imaging by PET and SPECT using labelled amino acids. Nuklearmedizin. 2011;50:167–73.
31. Herzog H, Langen KJ, Weirich C, Rota Kops E, Kaffanke J, Tellmann L, et al. High resolution BrainPET combined with simultaneous MRI. Nuklearmedizin. 2011;50:74–82.
32. Lohmann P, Herzog H, Rota Kops E, Stoffels G, Judov N, Filss C, et al. Dual-time-point O-(2-[(18)F]fluoroethyl)-L-tyrosine PET for grading of cerebral gliomas. Eur Radiol. 2015;25:3017–24.
33. Galldiks N, Stoffels G, Filss C, Rapp M, Blau T, Tscherpel C, et al. The use of dynamic O-(2-18F-fluoroethyl)-l-tyrosine PET in the diagnosis of patients with progressive and recurrent glioma. Neuro-Oncology. 2015;17:1293–300.
34. Rapp M, Heinzel A, Galldiks N, Stoffels G, Felsberg J, Ewelt C, et al. Diagnostic performance of 18F-FET PET in newly diagnosed cerebral lesions suggestive of glioma. J Nucl Med. 2013;54:229–35.
35. Pauleit D, Floeth F, Hamacher K, Riemenschneider MJ, Reifenberger G, Müller HW, et al. O-(2-[18F]fluoroethyl)-L-tyrosine PET combined with MRI improves the diagnostic assessment of cerebral gliomas. Brain. 2005;128:678–87.
36. Louis DN, Perry A, Reifenberger G, von Deimling A, Figarella-Branger D, Cavenee WK, et al. The 2016 World Health Organization classification of tumors of the central nervous system: a summary. Acta Neuropathol. 2016;131:803–20.
37. Felsberg J, Rapp M, Loeser S, Fimmers R, Stummer W, Goeppert M, et al. Prognostic significance of molecular markers and extent of resection in primary glioblastoma patients. Clin Cancer Res. 2009;15:6683–93.
38. Pöpperl G, Götz C, Rachinger W, Gildehaus FJ, Tonn JC, Tatsch K. Value of O-(2-[18F]fluoroethyl)-L-tyrosine PET for the diagnosis of recurrent glioma. Eur J Nucl Med Mol Imaging. 2004;31:1464–70.
39. Rachinger W, Goetz C, Pöpperl G, Gildehaus FJ, Kreth FW, Holtmannspotter M, et al. Positron emission tomography with O-(2-[18F]fluoroethyl)-l-tyrosine versus magnetic resonance imaging in the diagnosis of recurrent gliomas. Neurosurgery. 2005;57:505–11.
40. Mihovilovic MI, Kertels O, Hanscheid H, Lohr M, Monoranu CM, Kleinlein I, et al. O-(2-((18)F)fluoroethyl)-L-tyrosine PET for the differentiation of tumour recurrence from late pseudoprogression in glioblastoma. J Neurol Neurosurg Psychiatry. 2019;90:238–9.
41. Mehrkens JH, Pöpperl G, Rachinger W, Herms J, Seelos K, Tatsch K, et al. The positive predictive value of O-(2-[18F]fluoroethyl)-L-

tyrosine (FET) PET in the diagnosis of a glioma recurrence after multimodal treatment. J Neuro-Oncol. 2008;88:27–35.
42. Kebir S, Fimmers R, Galldiks N, Schafer N, Mack F, Schaub C, et al. Late Pseudoprogression in glioblastoma: diagnostic value of dynamic O-(2-[18F]fluoroethyl)-L-tyrosine PET. Clin Cancer Res. 2016;22:2190–6.
43. Langen KJ, Stoffels G, Filss C, Heinzel A, Stegmayr C, Lohmann P, et al. Imaging of amino acid transport in brain tumours: positron emission tomography with O-(2-[(18)F]fluoroethyl)-L-tyrosine (FET). Methods. 2017;130:124–34.
44. Melguizo-Gavilanes I, Bruner JM, Guha-Thakurta N, Hess KR, Puduvalli VK. Characterization of pseudoprogression in patients with glioblastoma: is histology the gold standard? J Neuro-Oncol. 2015;123:141–50.
45. Hutterer M, Nowosielski M, Putzer D, Jansen NL, Seiz M, Schocke M, et al. [18F]-fluoro-ethyl-L-tyrosine PET: a valuable diagnostic tool in neuro-oncology, but not all that glitters is glioma. Neuro-Oncology. 2013;15:341–51.
46. Filss CP, Galldiks N, Stoffels G, Sabel M, Wittsack HJ, Turowski B, et al. Comparison of 18F-FET PET and perfusion-weighted MR imaging: a PET/MR imaging hybrid study in patients with brain tumors. J Nucl Med. 2014;55:540–5.
47. Henriksen OM, Larsen VA, Muhic A, Hansen AE, Larsson HB, Poulsen HS, et al. Simultaneous evaluation of brain tumour metabolism, structure and blood volume using [(18)F]-fluoroethyltyrosine (FET) PET/MRI: feasibility, agreement and initial experience. Eur J Nucl Med Mol Imaging. 2016;43:103–12.
48. Göttler J, Lukas M, Kluge A, Kaczmarz S, Gempt J, Ringel F, et al. Intra-lesional spatial correlation of static and dynamic FET-PET parameters with MRI-based cerebral blood volume in patients with untreated glioma. Eur J Nucl Med Mol Imaging. 2017;44:392–7.
49. Zhang K, Langen KJ, Neuner I, Stoffels G, Filss C, Galldiks N, et al. Relationship of regional cerebral blood flow and kinetic behaviour of O-(2-(18)F-fluoroethyl)-L-tyrosine uptake in cerebral gliomas. Nucl Med Commun. 2014;35:245–51.
50. Stegmayr C, Schöneck M, Oliveira D, Willuweit A, Filss C, Galldiks N, et al. Reproducibility of O-(2-(18)F-fluoroethyl)-L-tyrosine uptake kinetics in brain tumors and influence of corticoid therapy: an experimental study in rat gliomas. Eur J Nucl Med Mol Imaging. 2016;43:1115–23.
51. Zhang H, Ma L, Shu C, Wang YB, Dong LQ. Diagnostic accuracy of diffusion MRI with quantitative ADC measurements in differentiating glioma recurrence from radiation necrosis. J Neurol Sci. 2015;351:65–71.
52. Bobek-Billewicz B, Stasik-Pres G, Majchrzak H, Zarudzki L. Differentiation between brain tumor recurrence and radiation injury using perfusion, diffusion-weighted imaging and MR spectroscopy. Folia Neuropathol. 2010;48:81–92.
53. Huang RY, Neagu MR, Reardon DA, Wen PY. Pitfalls in the neuroimaging of glioblastoma in the era of antiangiogenic and immuno/targeted therapy—detecting illusive disease, defining response. Front Neurol. 2015;6:33.
54. Sundgren PC, Fan X, Weybright P, Welsh RC, Carlos RC, Petrou M, et al. Differentiation of recurrent brain tumor versus radiation injury using diffusion tensor imaging in patients with new contrast-enhancing lesions. Magn Reson Imaging. 2006;24:1131–42.
55. Lohmann P, Werner JM, Shah NJ, Fink GR, Langen KJ, Galldiks N. Combined amino acid positron emission tomography and advanced magnetic resonance imaging in glioma patients. Cancers (Basel). 2019;11.
56. Sasaki M, Yamada K, Watanabe Y, Matsui M, Ida M, Fujiwara S, et al. Variability in absolute apparent diffusion coefficient values across different platforms may be substantial: a multivendor, multi-institutional comparison study. Radiology. 2008;249:624–30.
57. Ogura A, Tamura T, Ozaki M, Doi T, Fujimoto K, Miyati T, et al. Apparent diffusion coefficient value is not dependent on magnetic resonance systems and field strength under fixed imaging parameters in brain. J Comput Assist Tomogr. 2015;39:760–5.
58. Wu CC, Jain R, Radmanesh A, Poisson LM, Guo WY, Zagzag D, et al. Predicting genotype and survival in glioma using standard clinical MR imaging apparent diffusion coefficient images: a pilot study from the Cancer genome atlas. AJNR Am J Neuroradiol. 2018;39:1814–20.